

Research paper

Analysis of statistical characteristics of freak waves based on High Order Spectral coupled with CFD method

Yuan Zhuang^a, Yangjun Wang^b, Zhiben Shen^c, Guohua Pan^d, Decheng Wan^{a,*}

^a Computational Marine Hydrodynamics Lab (CMHL), School of Naval Architecture, Ocean and Civil Engineering, Shanghai Jiao Tong University, Shanghai, China

^b College of Advanced Interdisciplinary Studies, National University of Defense Technology, Nanjing, China

^c Hanjiang National Laboratory, Wuhan, China

^d Ningbo Pilot Station, Ningbo Dagang Pilotage Co., Ltd., Ningbo, China

ARTICLE INFO

Keywords:

Freak waves

Kurtosis and skewness

HOS-CFD coupled method

Nonlinear evolution process

ABSTRACT

Freak waves, which are characterized by their large wave heights and significant energy, can severely damage marine structures. The evolution of these freak waves is nonlinear, making it difficult to describe them with basic wave parameters. This paper analyzes the statistical characteristics of freak waves during the evolution. The freak waves are generated in a physical wave tank based on the two-wave train superposition method. An advanced coupled High-Order Spectral methods (HOS) and viscous Computational Fluid Dynamics (CFD) method is proposed to generate high quality freak waves. As the results of numerical methods agree well with the experimental results, the correlation between the statistical characteristics and freak wave mechanism is provided. The results reveal that the kurtosis of freak waves is related to the maximum wave crest, while the skewness is both influenced by the maximum wave height and the stream velocity at the wave crest. The wave propagation mechanisms are analyzed by Empirical Mode Decomposition (EMD). The results show that the location with the largest energy in low-frequency region sometimes occurs after the peak wave height, which may cause drift motion of floating structures and lead to hazards.

1. Introduction

In the past few decades, an increasing number of wrecked ships caused by freak waves have been recorded (Kjeldsen, 2004; Slunyaev et al., 2011). Some research institutions and researchers have observed and collected information on freak waves and found that the distribution of freak waves is extensive worldwide. With the growth of marine structures such platforms or wind turbines, the impact of freak waves on the stability and safety should be considered. Conventionally, freak waves were defined as those with a maximum wave height (H_{max}) exceeding twice the significant wave height (H_s), i.e., $H_{max} > 2H_s$ (Dysthe et al., 2008). However, freak waves exhibited high levels of randomness, asymmetry and nonlinearity. This complexity rendered the definition of traditional wave height and wave crest insufficient for fully characterizing their properties (Xue et al., 2023). Meanwhile, many studies focused on the certain peak wave height position when dealing with wave-structure interaction, neglecting other important positions. Therefore, by analyzing statistical characteristics and wave propagation

mechanisms, it may become possible to develop more accurate prediction models for freak wave-structure interaction.

Despite extensive research efforts on freak waves since the discovery of the Draupner wave in 1995 (Hayer and Andersen, 2000), there were still knowledge gaps. For instance, obtaining observed data on freak waves remained challenging (Ji et al., 2022). Some researchers have conducted freak waves reproduction in physical wave tanks. Deng et al. (2016) reproduced a freak wave in a physical wave tank by using the phase-amplitude iteration method. They discussed a secondary phase coupling between the harmonic components of freak waves. Ducroz et al. (2020) applied the time reversal (TR) method to reconstruct real-ocean freak waves in a physical wave tank. They provided a simple and accurate method for designing model-scale experiments. Luo et al. (2020) applied phase focusing method in the physical laboratory to generate freak waves. They concluded that high-peak freak waves would induce a large motion and high-frequency load of the TLP platform. These studies offer reference significance for the construction and research of freak waves. Nevertheless, their research failed to take into

* Corresponding author.

E-mail address: dcwan@sjtu.edu.cn (D. Wan).

URL: <http://dcwan.sjtu.edu.cn/> (D. Wan).

<https://doi.org/10.1016/j.oceaneng.2025.120615>

Received 19 December 2024; Received in revised form 29 January 2025; Accepted 4 February 2025

Available online 10 February 2025

0029-8018/© 2025 Elsevier Ltd. All rights are reserved, including those for text and data mining, AI training, and similar technologies.

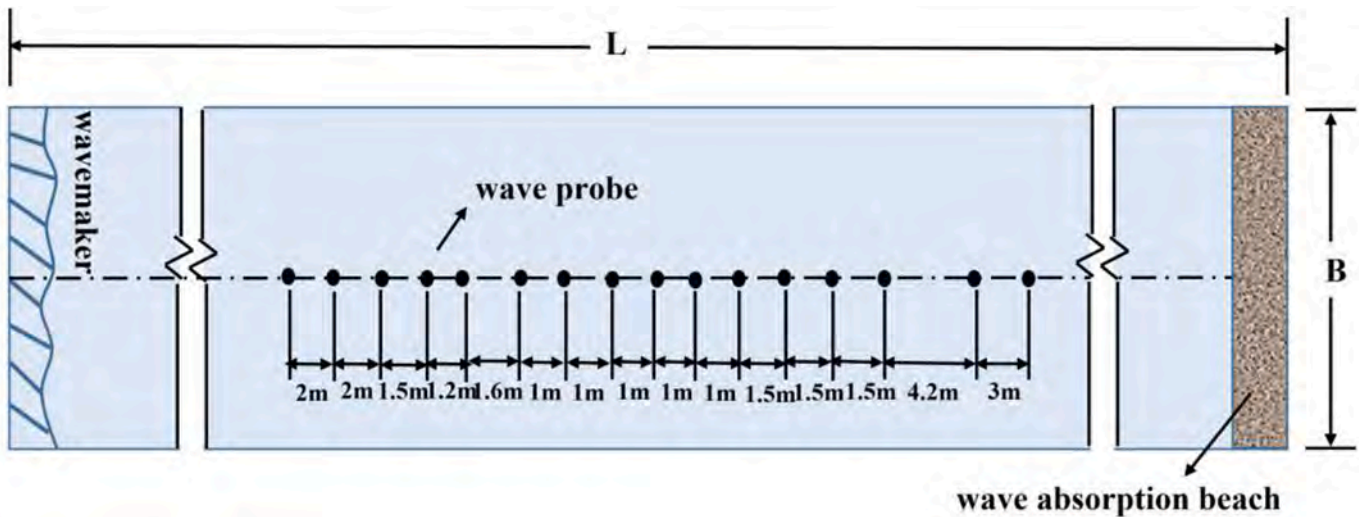


Fig. 1. The wave probes set-up in wave tank.

account the influence of statistical parameters.

Zou et al. (2019) considered the relationship between the freak wave factor (H_{max}/H_s , the ratio of the maximum wave height to the significant wave height) and kurtosis when freak waves passing through an isolated reef terrain in a wave tank. Abroug et al. (2022) found the kurtosis and skewness of focusing waves had an increasing trend with focusing process. Zhang et al. (2019) applied skewness and kurtosis to measure the deviation from the Gaussian process, which shows the strength of nonlinearity. Trulsen et al. (2020) studied a long-crested random waves propagating over a shoal, and demonstrated that the locations of maximum value of kurtosis and skewness were the same. These conclusions also coincided with those in constant wave steepness trains (Tian et al., 2011; Zeng and Trulsen, 2012; Mori et al., 2011). Wang et al. (2022) studied the correlation between the occurrence probability of freak waves and kurtosis/skewness. They pointed out that the occurrence probability of freak waves has a strong correlation with kurtosis. Those studies mentioned above indicated that the statistical characteristics were closely related to the features of freak waves. However, most of them were utilized to predict the possibility of the occurrence of freak waves, and the relationships between different statistical parameters and various factors influencing freak waves are not fully explored.

Based on the previous researches, many researchers have conducted numerical methods to generate and analyze freak waves. There were mainly two methods to reproduce freak waves, one is potential flow theory, the other is CFD method. For instance, Wang et al. (2023) applied a fully nonlinear high-order spectral method to conduct long-term simulations of multi-directional sea states. Deng et al. (2024) conducted numerical wave tank based on OpenFOAM source packets to reproduce specific freak wave. Both methods have their own advantages and disadvantages, and numerical methods were mostly used to study the interaction between freak waves and structures.

Many previous studies on the interaction between freak waves and structures have mainly focused on the peak position of the wave, overlooking the potential hazards in other positions. For instance, the marine structures encountered with freak waves may induce green water (Zhuang et al., 2023; Wang et al., 2023), violent sloshing phenomenon (Zhuang et al., 2022), significant dynamic responses and mooring line forces (Xu et al., 2024) and so on. However, existing studies have revealed that the location of the maximum wave height may not necessarily be the most perilous site. Zhao et al. (2014) demonstrated that maximum heave motion occurred when the body was placed distantly from the peak position. Chang et al. (2021) delineated the influence of the peak position of freak waves. Due to the second-order wave force was close to the natural period of the floating structure,

the second-order wave force is more essential for those structures. However, these studies only provided the results the impact of different positions of freak waves, the connection between freak waves and wave-structure interactions were not clear.

In order to figure out the nonlinear evolution of freak waves and how they affect the structures, we conducted the two-wave train superposition model and applied it in a physical wave tank to generate freak waves. There are two main methods for freak wave generation, linear and nonlinear. Linear methods are based on linear wave theory, including the "New wave" theory, wave train superposition model, and modified phase modulation model (Tromans et al., 1991; Kriebel and Alsina, 2000; Sun et al., 2008). They can create distinct freak waves in numerical wave tanks, facilitating the study of wave - structure interactions. Nonlinear methods, such as breather - type methods, NLS - type methods, and HOS - WG method, focus on nonlinear wave interactions (Chabchoub et al., 2011; Khaït, 2020; Houtani et al., 2015). The advantage of linear methods is that they allow for convenient examination of the interaction between freak waves and structures due to their ability to generate specific waves, which simplifies the research process. Sixteen wave probes were displaced to analyze the evolution of freak waves. The potential theory (High-Order Spectral Method, short for HOS) and viscous Computational Fluid Dynamics (CFD) coupled method (short for HOS-CFD) were used to perform the numerical analysis. The HOS method has the characteristics of high efficiency and accuracy in the generation of freak wave problems. It is extended from Zakharov equation to a higher steepness wave, which is one of the most perfect models in dealing with freak waves. However, the HOS method cannot consider the viscosity such as breaking wave phenomenon. Therefore, we couple HOS with CFD methods to preserve the characteristics of HOS to generate freak waves quickly and accurately, while considering the viscous effects. Simultaneously, because the freak waves have been completely obtained in the HOS region, we can reduce the computational area and computational time of the CFD without considering the space and time required for the generation and evolution of the freak waves. The experimental setup and numerical methods are presented in Section 2. In Section 3, the experimental results are carried out and these two methods are validated. In Section 4, the statistical characteristics of freak waves are analyzed. The nonlinear evolution of freak waves was considered based on wavelet analysis and Empirical Mode Decomposition (EMD).

Table 1

Main parameters in test cases.

ID	T_P (s)	H_S (m)
CASE1	1.74	0.10
CASE2	1.95	0.15

2. Methodology

2.1. Two-wave train superposition model

The experimental freak wave generation is based on a two-wave train superposition model (Kriebel and Alsina, 2000). The mathematical expression is described below:

$$\eta(x, t) = \sum_{n=1}^N A_{1n} \cos(k_n x - \omega_n t - \varepsilon_n) + \sum_{n=1}^N A_{2n} \cos(k_n(x - x_c) - \omega_n(t - t_c)) \quad (1)$$

$$A_{1n} = \sqrt{2P_1 S(\omega_n) \delta_{\omega n}} \quad (2.a)$$

$$A_{2n} = \sqrt{2P_2 S(\omega_n) \delta_{\omega n}} \quad (2.b)$$

$$P_1 + P_2 = 1 \quad (2.c)$$

The two-wave train superposition model generates a freak wave by combining a random irregular wave and modulated focusing wave. The subscripts 1 and 2 represent random and focused waves, respectively. A is the composition wave amplitude, while k_n , ω_n and ε_n are wave number, circular frequency and initial phase of each wave component, respectively. The modulated focusing wave reaches the maximum wave height at position x_c and time t_c . $\delta_{\omega n}$ is the frequency interval of the energy spectrum. Parameters P_1 and P_2 are the ratios of the energy in the wave spectrum. The irregular wave acts as a background wave and the focusing wave controls the position and time of freak wave generation. To guarantee freak wave generation, P_1 is chosen to be 0.95, whereas P_2 is set to 0.05. After generating the wave model through the two-wave train superposition model, a Fast Fourier Transform method is applied to obtain the wave components before the wave generator in the physical wave tank.

2.2. Experimental set-up

The experiments are conducted in the towing tank of Marine Design

and Research Institute of China with 280m long, 10m wide and 5m deep. The towing tank is equipped with a flap-type wave generator. As shown in Fig. 1, sixteen wave probes are set up in the wave tank, located at $x = 49.7\text{m}, 51.7\text{m}, 53.7\text{m}, 55.2\text{m}, 56.4\text{m}, 58.0\text{m}, 59.0\text{m}, 60.0\text{m}, 61.0\text{m}, 62.0\text{m}, 63.0\text{m}, 64.5\text{m}, 66.0\text{m}, 67.5\text{m}, 72.1\text{m},$ and 75.1m away from the boundary of the wave tank, respectively. The two types of freak waves are constructed with different significant wave heights and spectrum peak periods, the main parameters of these two waves are shown in Table 1. The process of freak wave generation in physical wave tank is depicted in Fig. 2, combining two wave train superposition model and wave reproduction in physical wave tank.

2.3. Numerical method

In this study, we adopt a novel numerical method to analyze freak waves. The High-Order-Spectral (short for HOS) method is adopted to reproduce freak waves. In order to comply with the physical wave generation in the water tank, we use HOS-NWT (Ducrozet et al., 2006) for calculation. We coupled HOS with SJTU in-house solver naoe-FOAM-SJTU (Zhuang and Wan, 2021), which is a viscous solver developed based on the open-source software OpenFOAM. We first use the HOS method to reconstruct the waves in the wave tank, and subsequently apply the coupled HOS-CFD method to reproduce the waves at a specific location during a specific time period to reduce the viscous computational domain and calculated time.

HOS is a pseudo-spectral method and has advantages for solving nonlinear wave equations. The free surface elevation $\eta(\mathbf{x}, t)$ and surface potential $\phi^s(\mathbf{x}, t) = \phi(\mathbf{x}, \eta, t)$ can be defined as:

$$\frac{\partial \eta}{\partial t} = (1 + |\nabla \eta|^2) \frac{\partial \phi}{\partial z} - \nabla \phi^s \cdot \nabla \eta \quad (3)$$

$$\frac{\partial \phi^s}{\partial t} = -g\eta - \frac{1}{2} |\nabla \phi^s|^2 + \frac{1}{2} (1 + |\nabla \eta|^2) \left(\frac{\partial \phi}{\partial z} \right)^2 \quad (4)$$

The symbols t and z represent the time and the vertical axes, respectively. ∇ is the horizontal gradient. ϕ^s can be obtained by expanding ϕ in a perturbation series and evaluating each order of ϕ on free surface in Taylor series.

The governing equations of viscous domain are Navier-Stokes equations:

$$\nabla \cdot \mathbf{U} = 0 \quad (5)$$

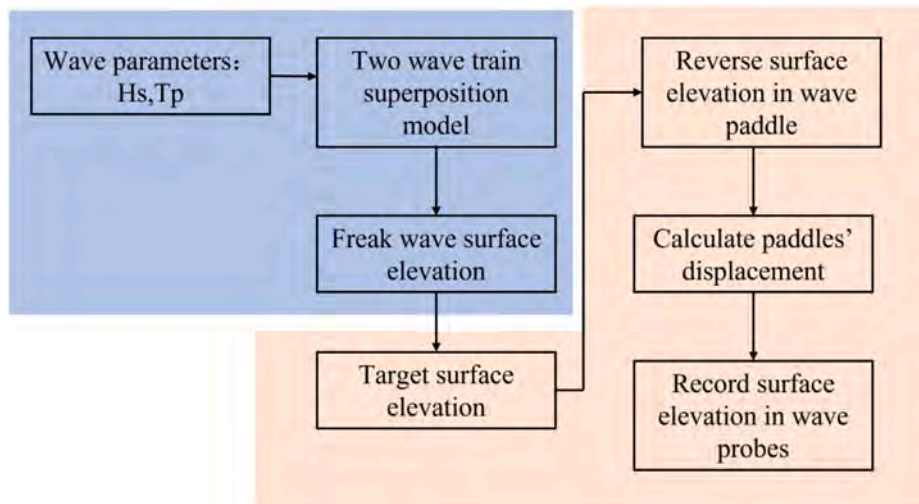


Fig. 2. Flowchart of the wave generation (orange background) based on two-wave train superposition model (blue background) in physical wave tank. (For interpretation of the references to colour in this figure legend, the reader is referred to the Web version of this article.)

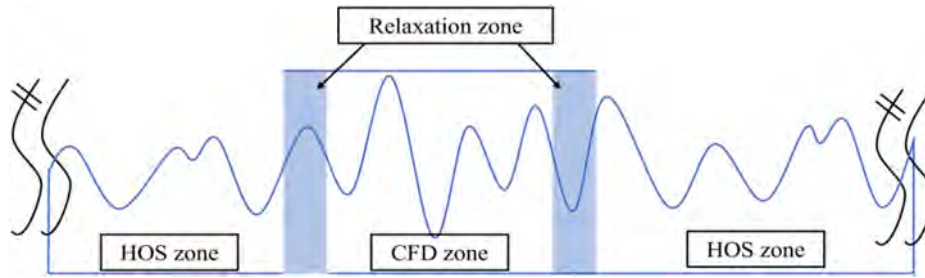


Fig. 3. The coupled scheme in HOS-CFD method.

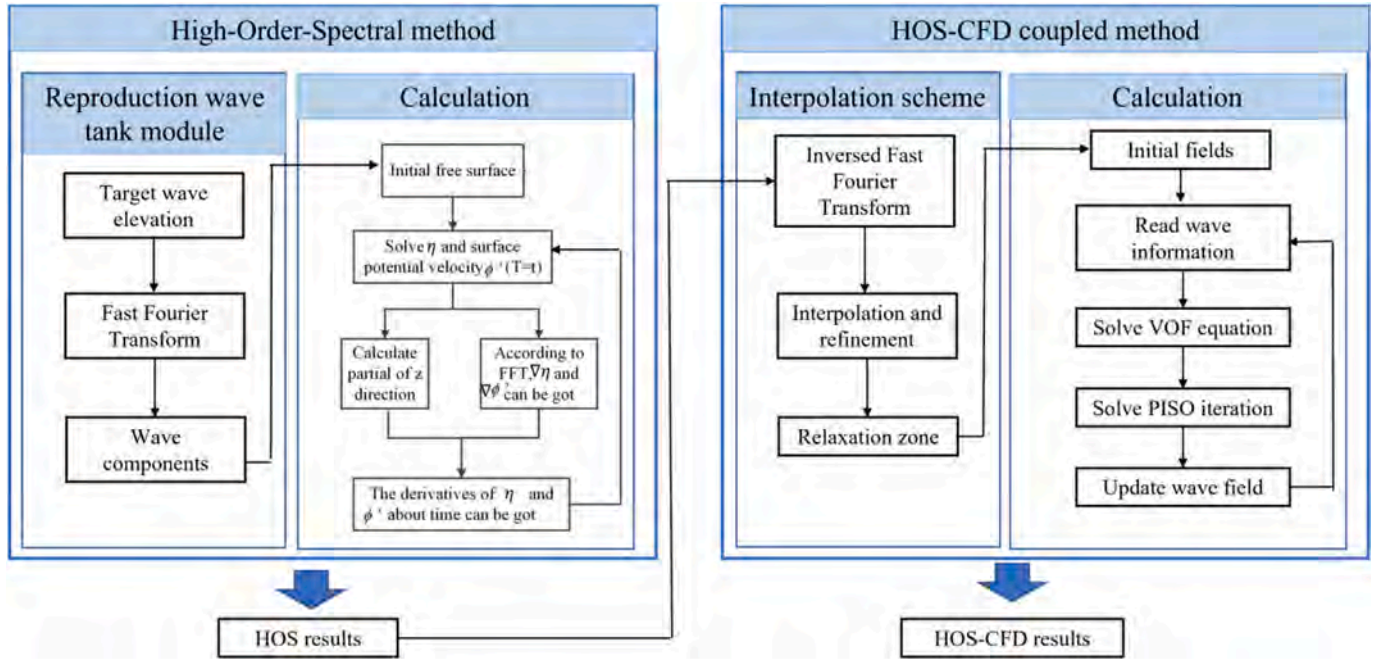


Fig. 4. The numerical method and calculation process.

$$\frac{\partial \rho \mathbf{U}}{\partial t} + \nabla \cdot (\rho \mathbf{U} \mathbf{U}) = -\nabla p_d - \mathbf{g} \cdot \mathbf{x} \nabla \rho + \nabla \cdot (\mu_{eff} \nabla \mathbf{U}) + (\nabla \mathbf{U}) \cdot \nabla \mu_{eff} + f_\sigma \quad (6)$$

where \mathbf{U} is the velocity field, $p_d = p - \rho \mathbf{g} \cdot \mathbf{x}$ is dynamic pressure, \mathbf{x} stands for the vector of the volumetric center position in cell; $\mu_{eff} = \rho(\nu + \nu_t)$ is effective dynamic viscosity, ρ is the density of the fluid, ν represents kinematic viscosity and ν_t is eddy viscosity. f_σ is the surface tension term in the two-phase flow model. The symbol t and ∇ mean the time and the horizontal gradient, respectively.

The details of coupled HOS-CFD method can be found in previous work (Zhuang et al., 2023). The scheme of relaxation zone is applied for coupling HOS and CFD method, as illustrated in Fig. 3. In this study, we add a reproduced wave-generation module to match the wave field created by a physical wave tank. The wave elevation is obtained from a certain position in wave tank, and then Fast Fourier Transform is applied to generate wave components. The two numerical methods and the computational flow used in this study are shown in Fig. 4.

3. Experimental and numerical results

3.1. Experimental results

Fig. 5 illustrates the comparison of the wave elevation at the typical positions of the repeatability test for the two freak wave conditions. The aim of the repeatability test is to confirm that the wave tank

environment has little influence on the results. The typical positions are chosen as $x = 59.0\text{m}$ in CASE 1 and $x = 62.0\text{m}$ in CASE2. It can be seen that the results of the two tests for each condition are in good agreement, which further indicates that the freak waves generated in the experiments have good repeatability. Table 2 shows the relative deviation of the statistical results at the typical locations of the repeatability test for two freak wave conditions. It can be seen that the relative deviation of the wave height, the occurrence time, and the significant wave height is less than 5%, which indicates that the freak wave generated in the experiment has good repeatability.

Fig. 6 shows the maximum wave height in CASE1 and CASE2. The ratio of the maximum wave height to the significant wave height near the target position $x = 60\text{m}$ in CASE1 case can reach up to 2.7, which satisfies the definition requirements of freak waves. The maximum wave height of CASE2 is 0.32m and formed at $x = 66\text{m}$, and the ratio of the maximum wave height to the sense wave height can reach up to 2.4, which meets the definition requirements of freak waves.

3.2. Comparison between numerical test and experiment

Before the numerical calculation, it is necessary to analyze the computational parameter settings for HOS and HOS-CFD coupling methods. Ducroz et al. (2012) explored and analyzed the computational parameters of HOS, and concluded that for strongly nonlinear waves, the order should not to be smaller than 5. For the freak wave calculation, a more detailed calculation setting was not provided. In

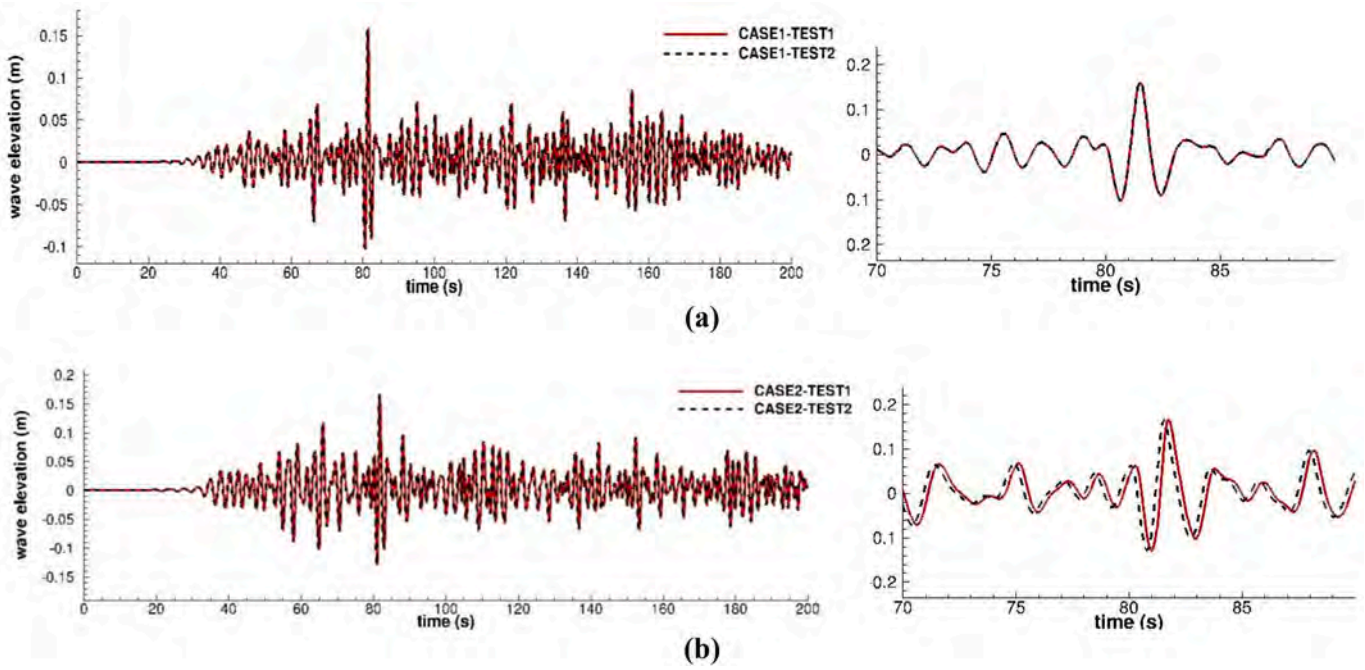


Fig. 5. The comparison of wave elevation in repeatability experiments: (a) CASE1, (b) CASE2.

Table 2

Relative error of replicate experiments in typical positions.

Case		Hmax		Time of Hmax happens		Hs	
		Value (m)	Relative error	Value (s)	Relative error	Value (m)	Relative error
CASE1	Test 1 (x = 59.0m)	0.261	0.77%	81.5	0.37%	0.105	0.95%
	Test 2 (x = 59.0m)	0.259		81.2		0.104	
CASE2	Test 1 (x = 62.0m)	0.290	0.69%	82.1	0.37%	0.142	4.23%
	Test 2 (x = 62.0m)	0.288		81.8		0.136	

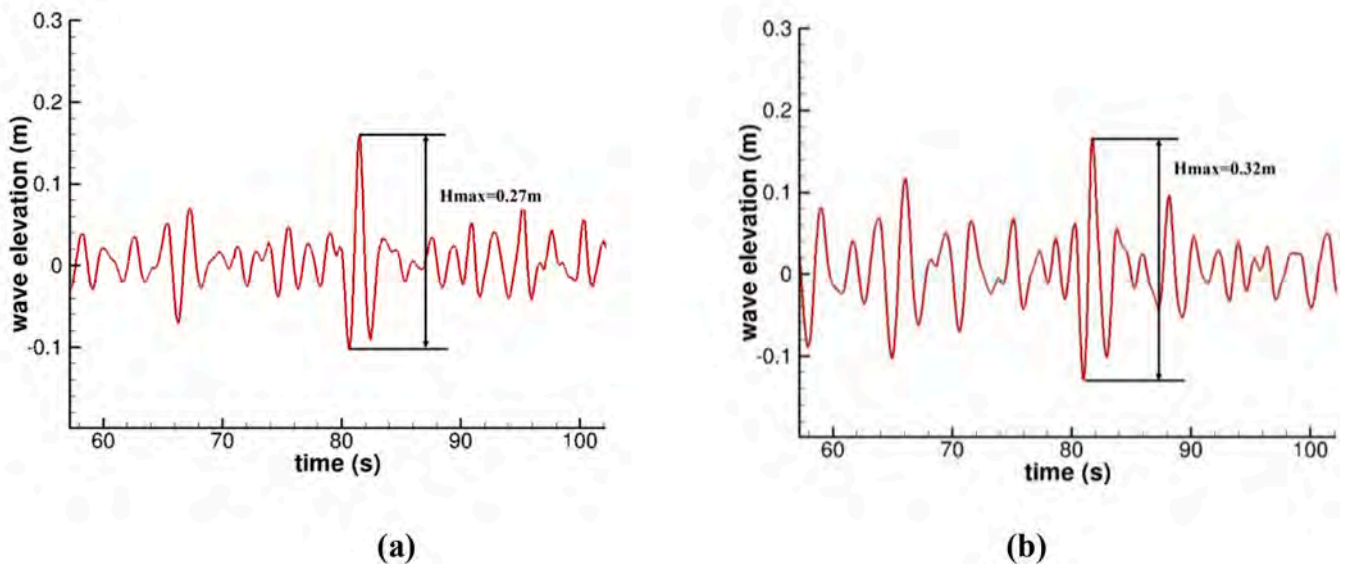


Fig. 6. The maximum wave height in the freak wave cases. (a) CASE1, (b) CASE2.

addition, we have discussed the parameter settings for nonlinear regular wave computation using HOS-CFD in our previous work (Zhuang and Wan, 2021), and it is also necessary to provide the corresponding

computational parameter settings for the computation of freak waves.

Fig. 7 illustrates the node and order study of HOS with freak parameters in CASE1. The black solid line represents the results of left

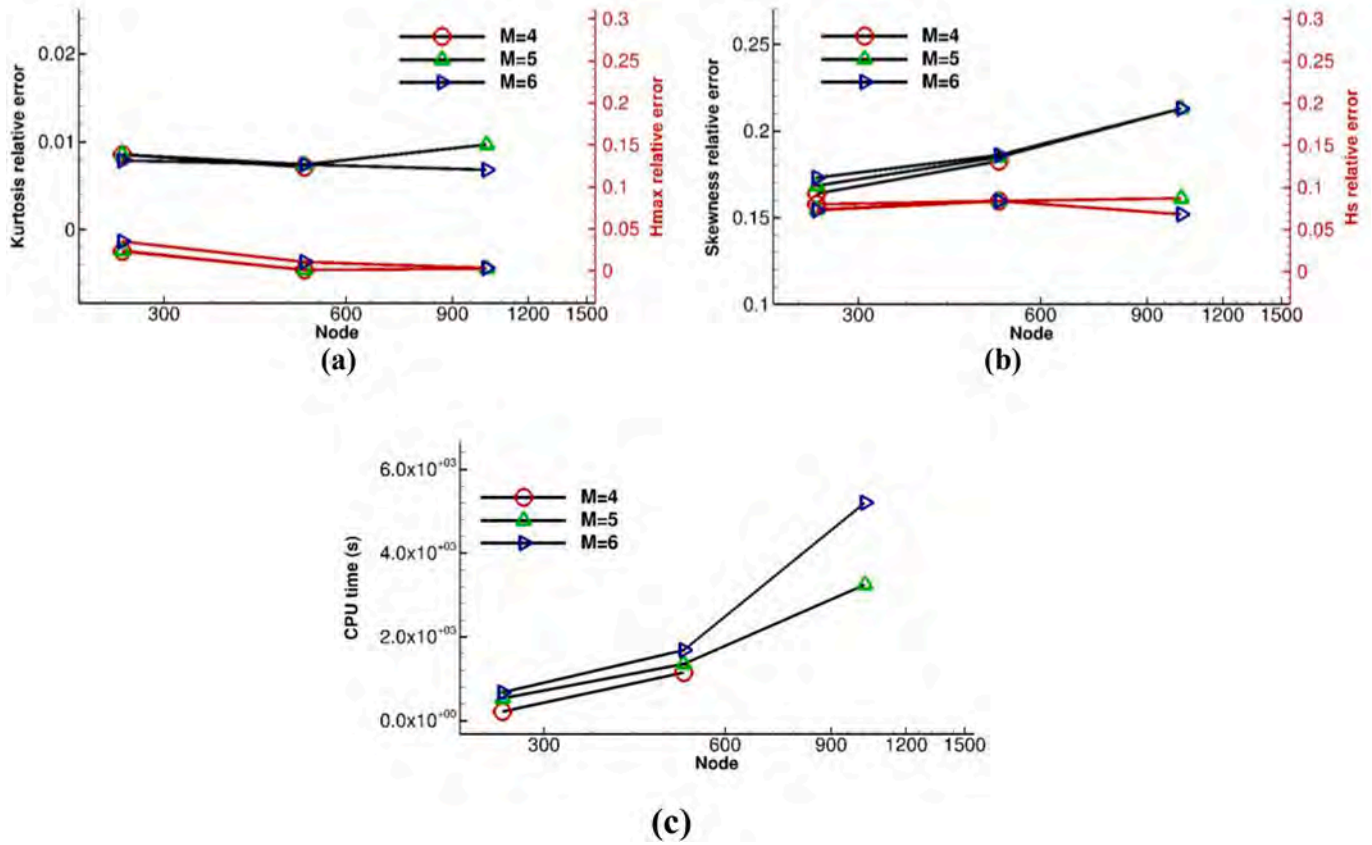


Fig. 7. The study of correlation among nodes, orders and freak parameters (a) kurtosis and Hmax, (b) skewness and Hs, (c) CPU time of CASE1.

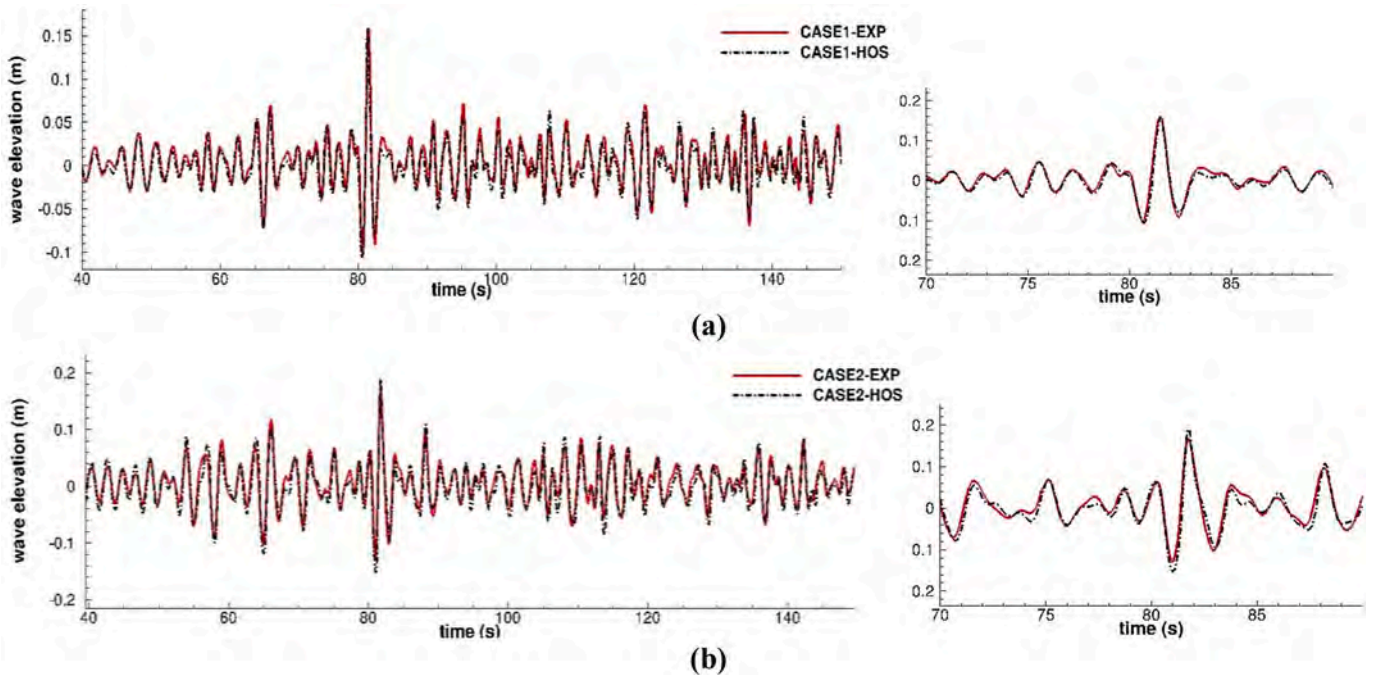


Fig. 8. The comparison between experiments and HOS in (a) wave elevation of CASE 1, (b) wave elevation of CASE 2.

coordinate axis and the red solid line represents the results of right coordinate axis. The kurtosis and skewness are the parameters to describe the statistical characteristics of freak waves. The detailed description and equation of these parameters can be found in Section 4. H_{max} in

Fig. 7 represents the value of maximum wave height, while H_s is the significant wave height of the freak wave. In this paper, three orders of HOS ($M = 4, 5, 6$) and three values of the number of nodes (Nodes = 256, 512, 1024) are discussed. The selection of the order has little effect

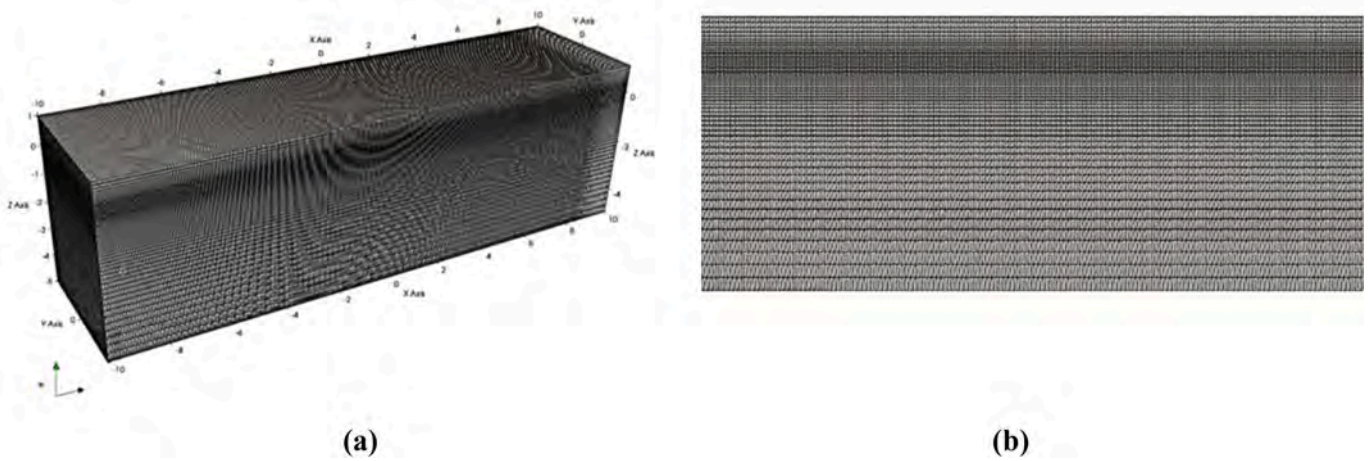


Fig. 9. The setup of (a) computational domain of viscous zone and (b) mesh generation.

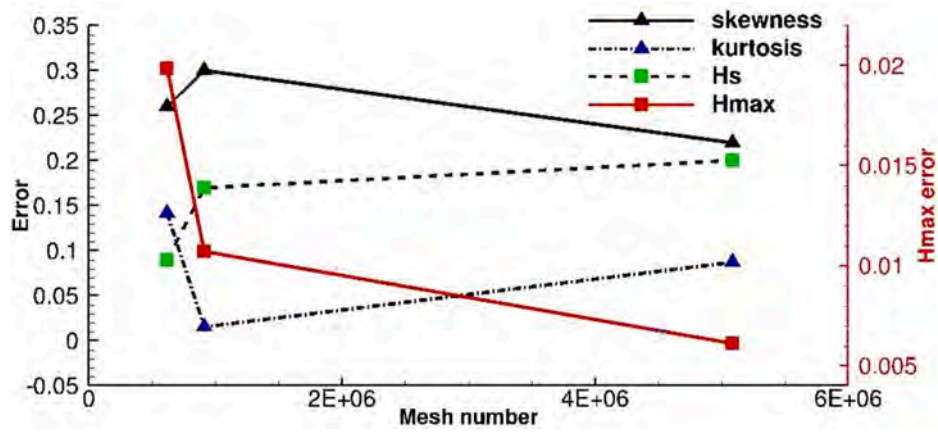


Fig. 10. The study of correlation between mesh, freak parameters and wave height of CASE1 in coupled method.

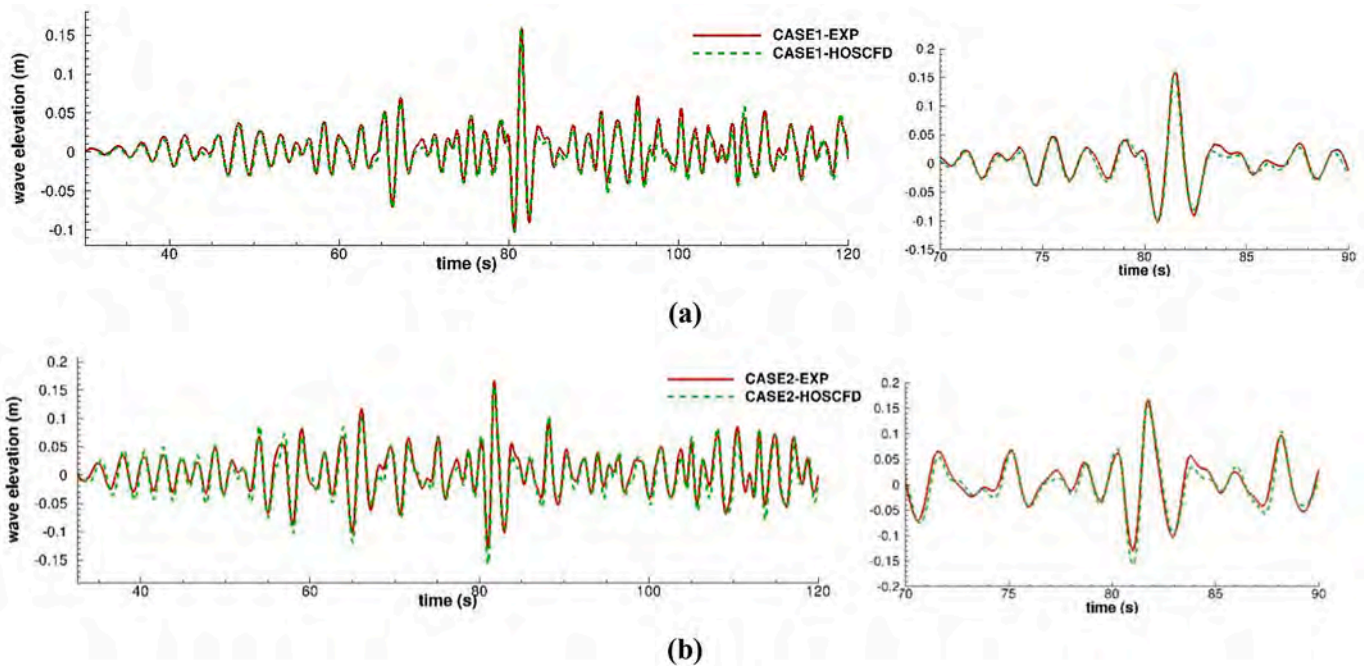


Fig. 11. The comparison of wave elevation between experiments and HOS-CFD coupled method in (a) CASE 1, (b) CASE 2.

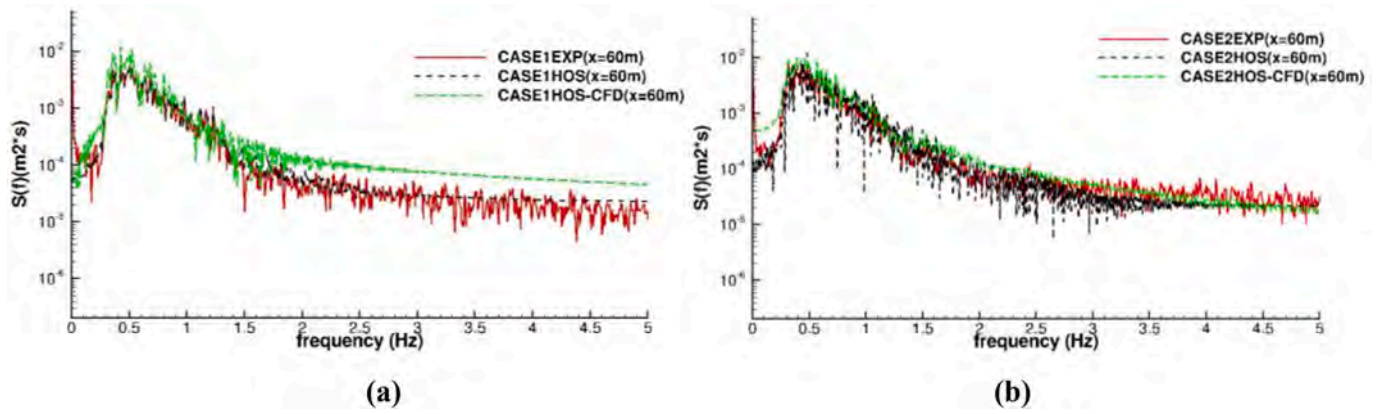


Fig. 12. The comparison of wave spectrum between experiments and HOS-CFD coupled method in (a) CASE 1, (b) CASE 2.

on the wave height and statistical parameters, while a significant increase in the CPU time is observed when $M = 6$. When the number of nodes increases, the errors of the maximum wave height and significant wave height with the experimental data gradually decrease, while the errors of skewness show a tendency to increase. The kurtosis error for M

$= 5$ also shows an increasing trend. The node represents the choice of discretization in x -direction, which defines the largest wavenumber that can be solved. The order of HOS corresponds to the nonlinear wave-wave interaction. Therefore, the increase in these two parameters will strengthen the influence of wave components with smaller wavelengths

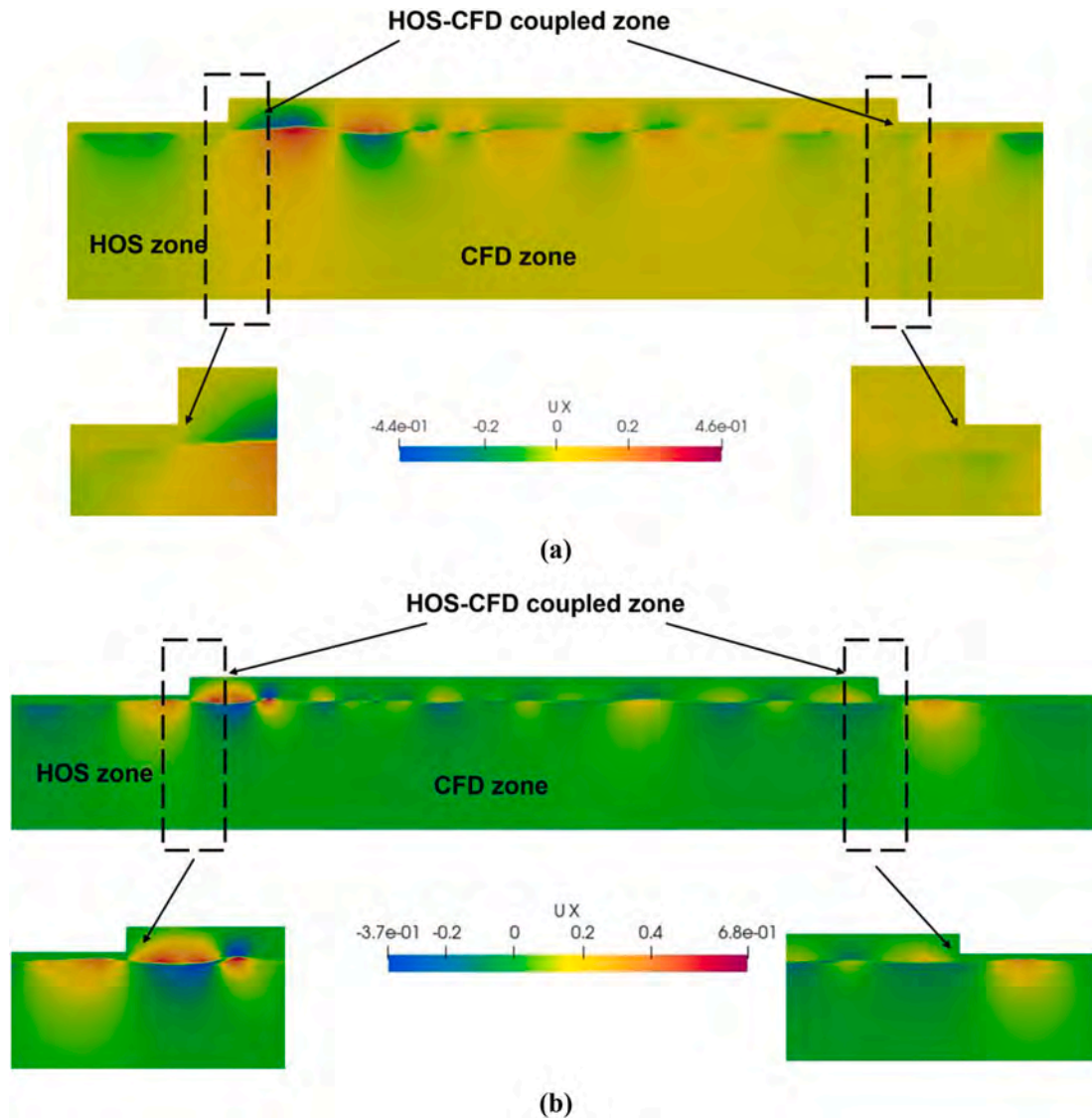


Fig. 13. The surface velocity of HOS-CFD coupled method in (a) CASE 1, (b) CASE 2.

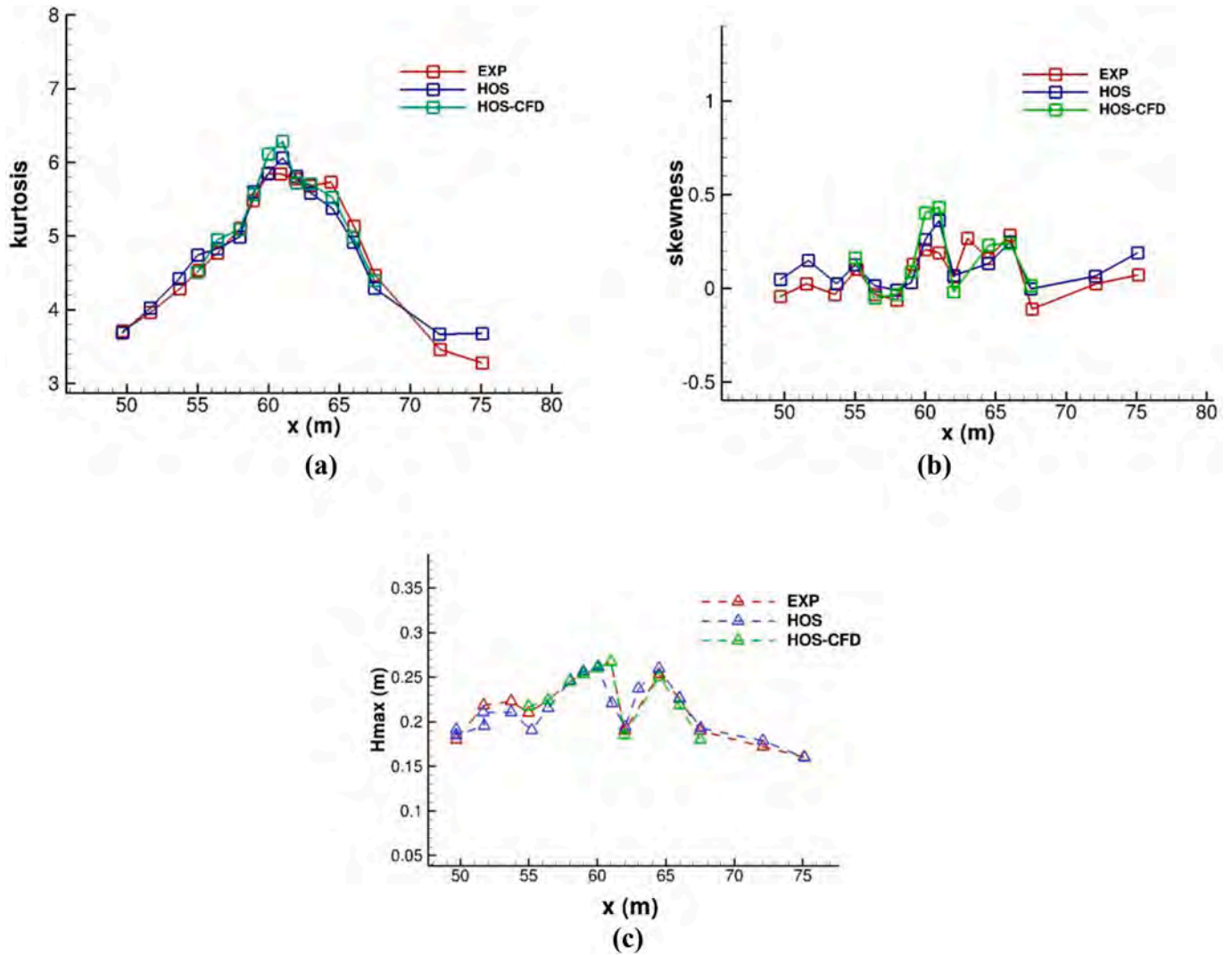


Fig. 14. The freak parameters (a) kurtosis, (b) skewness and (c) H_{max} of CASE1.

and wave-wave interactions in wave propagation. Meanwhile, the value of skewness and kurtosis reveals the deviation of the Gaussian distribution. As the number of orders and nodes increases, the simulation of nonlinear terms of the wave becomes more precise. Nevertheless, the increase in the number of orders and nodes also leads to an escalation in the nonlinearity of the wave evolution, thereby resulting in a heightened statistical error in the overall wave field. In order to explore the statistical values of the freak waves and reduce the CPU time, the parameters are chosen to be $M = 5$ and $\text{Nodes} = 512$ for HOS simulation.

The comparisons between the results of numerical simulations and experimental data are shown in Fig. 8. The time histories of both the wave elevation and the wave spectrum are compared. It can be seen that the results of HOS agree well with the experimental data.

After validating the freak waves in HOS method, the wave elevation in HOS-CFD method is estimated. We analyze the errors of wave heights and statistical parameters compared to the experiments using three grid generations. We apply the suitable parameters with 86 mesh grids per wavelength, 10 mesh grids per wave height for coarse mesh generation. The total number of these three types of grid mesh is 0.61 million, 0.91 million and 5.08 million, respectively. The size of the CFD domain is $-10\text{m} < x < 10\text{m}$, $-2.5\text{m} < y < 2.5\text{m}$, $-5\text{m} < z < 1\text{m}$, as shown in Fig. 9. The duration of the time window is chosen to be 30s–120s, therefore the actual simulation time of the coupled method is 90s.

The errors between the experimental data and the coupled method

are shown in Fig. 10. The left-hand coordinates indicate the errors in the statistical parameters and significant wave height, while the right-hand coordinates represent the errors in the maximum wave height. The figure illustrates that the optimal settings for the maximum wave height and skewness are associated with a fine grid, whereas the ideal settings for kurtosis and significant wave height are medium and sparse grids, respectively. However, the error of the maximum wave height between the medium and fine meshes is approximately 0.5%, which can be ignored considering the calculation time. Therefore, the medium mesh is selected for the subsequent simulation.

Fig. 11 illustrates the wave elevation between the coupled method and the experimental results. The results show a good agreement between numerical data and experimental data both in amplitude and phase. The wave spectrum of experimental and HOS-CFD method is compared in Fig. 12. The CASE 2 has good agreement while CASE 1 has discrepancies in high frequency in HOS-CFD method. This may be due to a smaller computational time in HOS-CFD method, giving the discrepancy in wave spectrum.

The velocity in HOS-CFD method is depicted in Fig. 13. The connection between HOS zone and CFD zone is enlarged separately. It can be seen that around the coupled zone, the continuity of velocity in free surface keeps well. After validating the method and numerical results, the analysis of freak waves can be performed numerically.

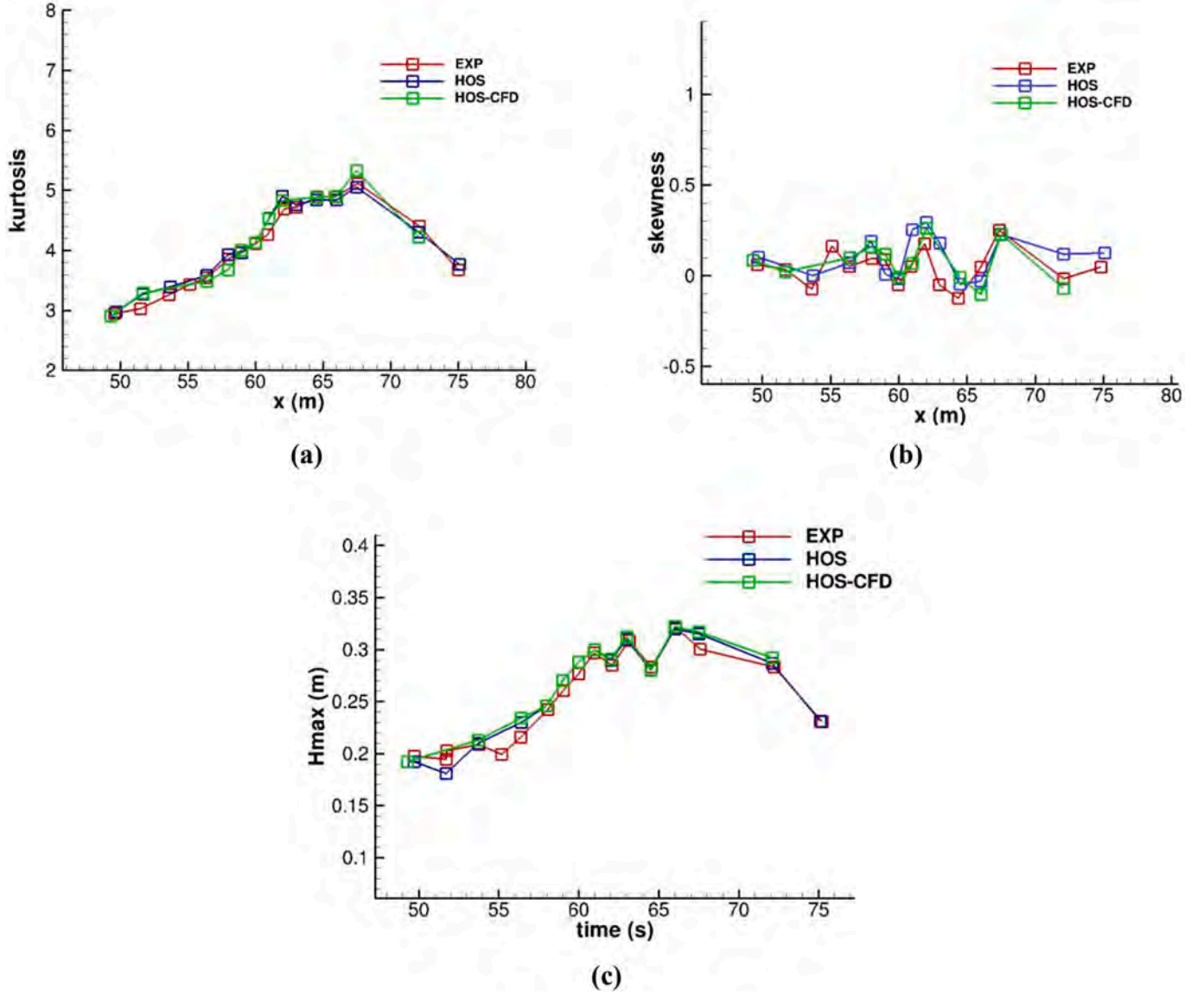


Fig. 15. The freak parameters (a) kurtosis, (b) skewness and (c) H_{max} of CASE2.

4. Numerical analysis and discussion

4.1. Numerical analysis of kurtosis and skewness

Conventional waves are considered as standard stochastic processes, but freak waves are subject to nonlinearity. As a result, the distribution of freak wave processes differs from the Gaussian distribution, and this deviation can be assessed using skewness and kurtosis.

Kurtosis can be illustrated as (Mori and Janssen, 2006):

$$\beta_2 = \frac{1}{\eta_{rms}^4} \frac{1}{N} \sum_{n=1}^N (\eta_n - \bar{\eta})^4 \quad (7)$$

Skewness can be described as (Mori and Janssen, 2006):

$$\sqrt{\beta_1} = \frac{1}{\eta_{rms}^3} \frac{1}{N} \sum_{n=1}^N (\eta_n - \bar{\eta})^3 \quad (8)$$

where N is the number of measurement points of wave surface elevation, η_{rms} is the root-mean-square value of the wavefront elevation at each measurement point, η_n is the wave surface elevation at the n th measurement point, and $\bar{\eta}$ is the average value of the wave surface elevation

at each measurement point. In the case of the Gaussian distribution, the values of skewness $\sqrt{\beta_1}$ and kurtosis β_2 are 0 and 3.0. Under real-world sea conditions, the wave profile is typically asymmetrical, featuring steep peaks and gentle troughs in the vertical direction, with the value of the wave crest being greater than that of the wave trough. In the horizontal direction, the front slope is steeper than the back slope near the broken waves. Therefore, the skewness can be utilized as a composite measure of this asymmetry.

Fifteen wave probes are set up in the numerical wave tank, located at $x = 49.7\text{m}$, 51.7m , 53.7m , 56.4m , 58.0m , 59.0m , 60.0m , 61.0m , 62.0m , 63.0m , 64.5m , 66.0m , 67.5m , 72.1m , and 75.1m away from the inlet of the numerical wave tank, respectively. Figs. 14 and 15 show kurtosis, skewness and maximum wave height of CASE 1 and CASE 2 at different measurement points respectively. The time history of wave height in numerical simulations align well with the experimental data. Nonetheless, the kurtosis and skewness values measured at some wave probes are slightly greater than the experimental values. Despite this discrepancy, the overall trend remains consistent with the experimental data.

As depicted in Fig. 14, the peak wave height in CASE 1 is observed at $x = 60\text{m}$, and the greatest value of kurtosis happens at $x = 61\text{m}$. Moreover, CASE 1 demonstrates a secondary maximum wave height at x

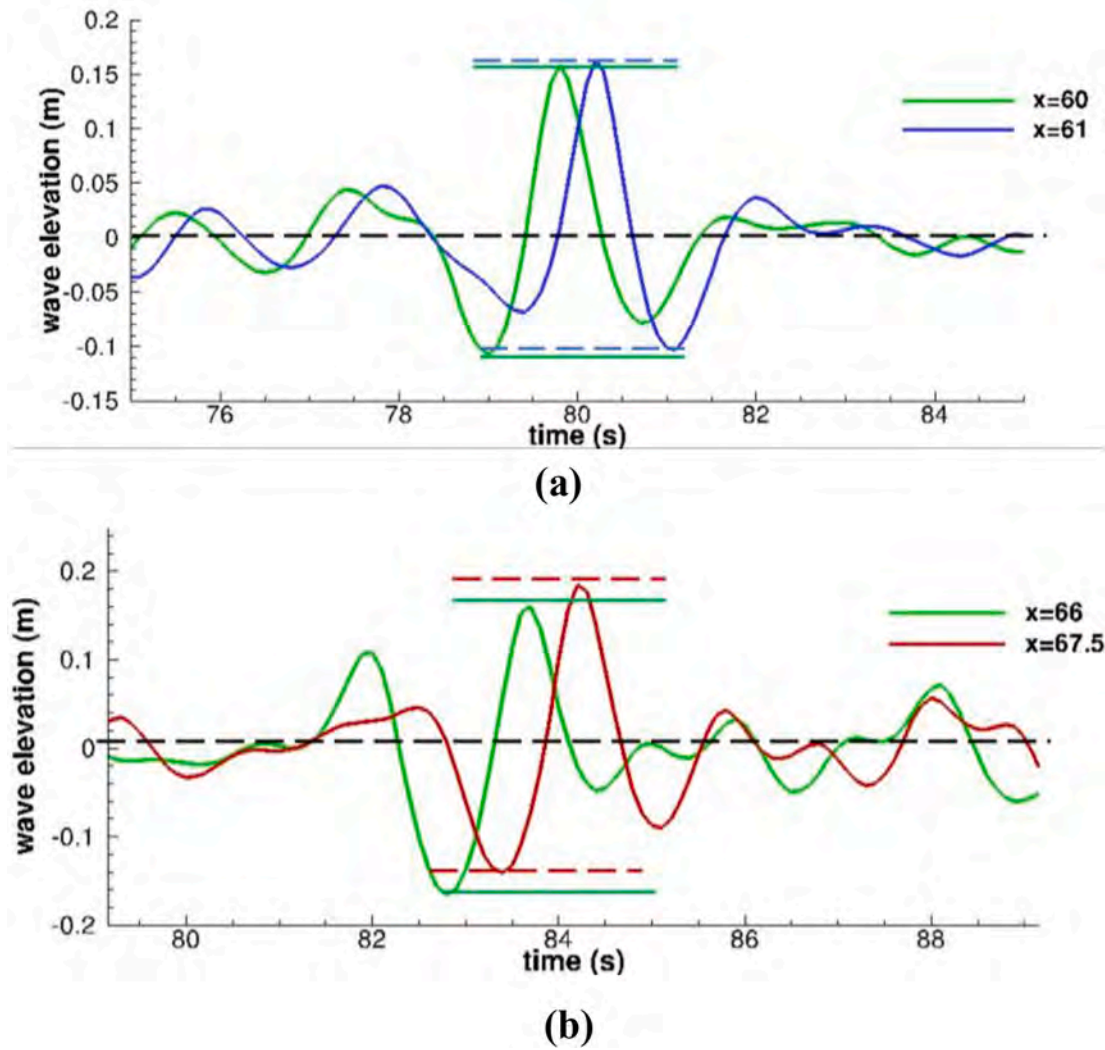


Fig. 16. The comparison of surface elevation between maximum wave height position and maximum kurtosis value position in (a) CASE1, (b) CASE2.

= 64.5m, which shows a sudden increase in the kurtosis value. This pattern is also evident in CASE 2, as illustrated in Fig. 15. The maximum wave height of CASE 2 occurs at $x = 66$ m, and the kurtosis value reaches its peak at $x = 67.5$ m. Additionally, at $x = 64.5$ m, there is a secondary peak of the maximum wave height, and the kurtosis value curve exhibits a pronounced peak as well. It seems that the trend of the kurtosis reveals the value of largest wave height, for it increases with the rise of the largest wave height in different positions. However, it seems that the largest value of kurtosis happens after the peak wave height position.

Fig. 16 illustrates the comparison of surface elevation between the position of maximum wave height and the maximum kurtosis value. The surface elevation at $x = 61$ m (CASE1) and $x = 67.5$ m (CASE2) exhibits a larger wave crest than those at the maximum wave height position ($x = 60$ m in CASE1 and $x = 66$ m in CASE2). The value of kurtosis is more closely to the value of wave crest other than the wave height.

The correlation between skewness and maximum wave height is not singular. Although there is a clear prominent value in skewness at the location of the maximum wave height, several peak values still exist in

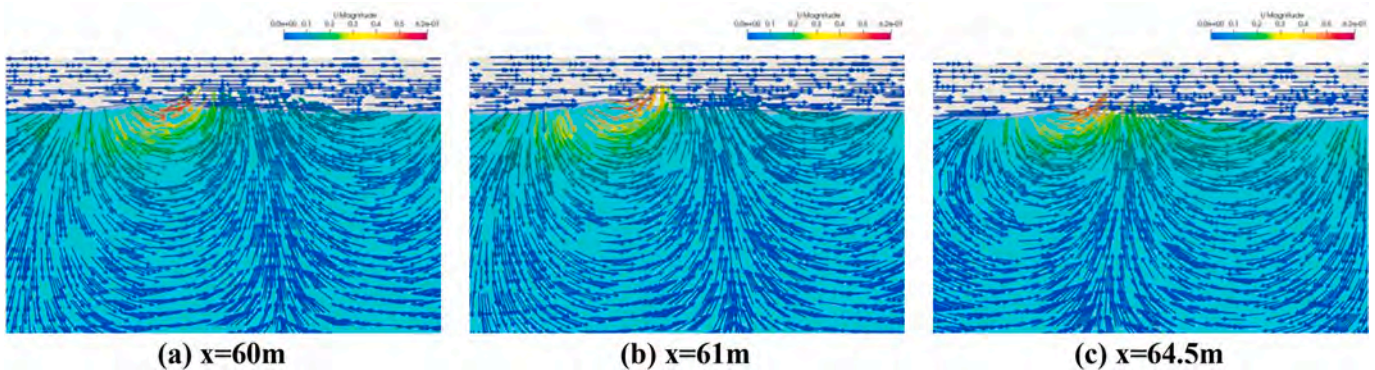


Fig. 17. The stream velocity propagation of wave field in CASE 1.

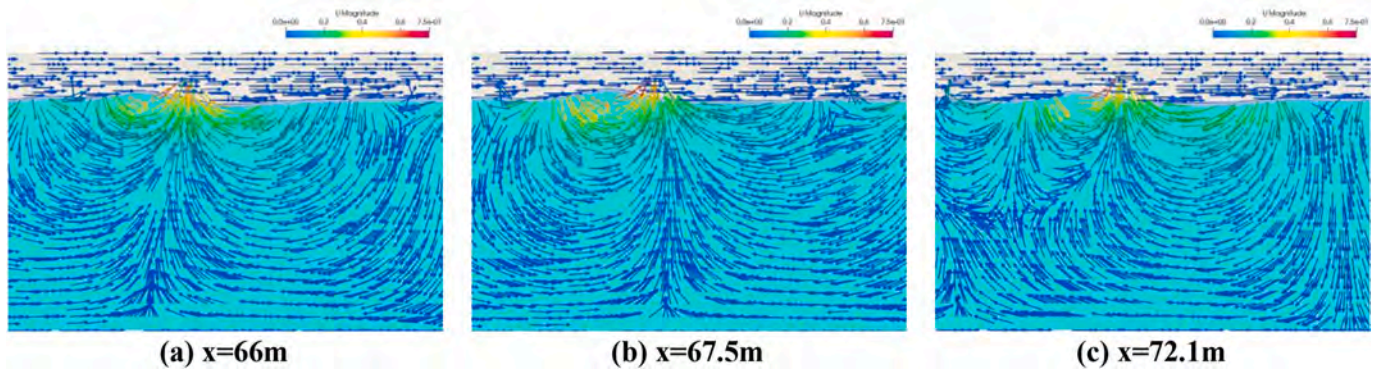


Fig. 18. The stream velocity propagation of wave field in CASE 2.

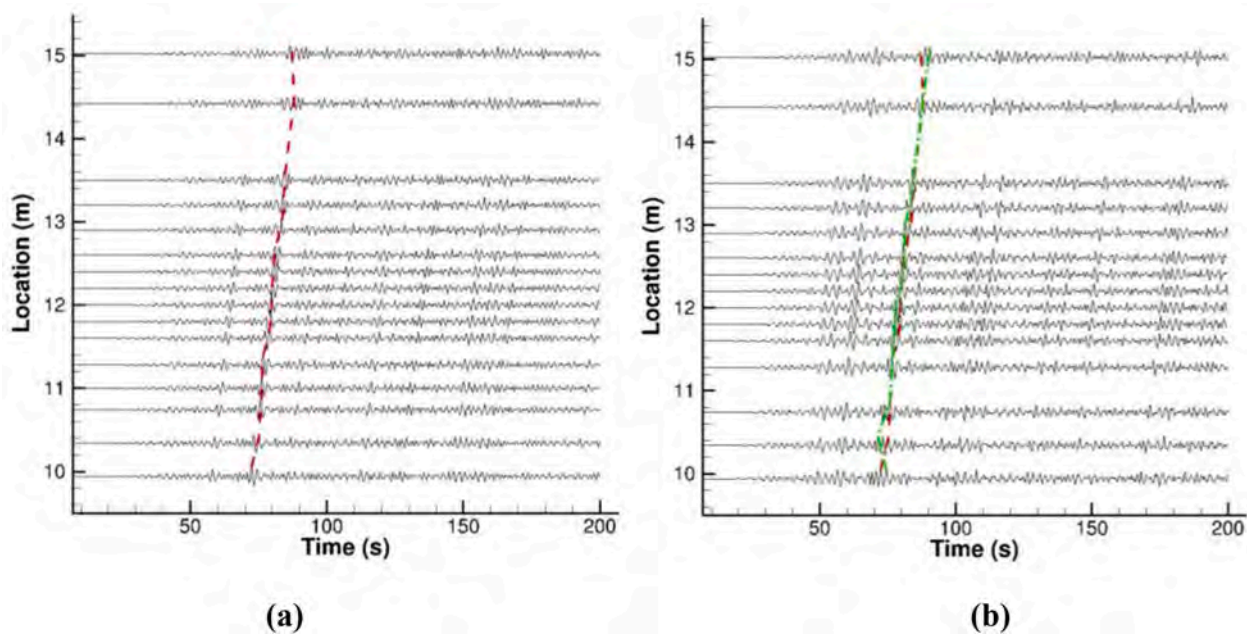


Fig. 19. The wave evolution process in CASE 1 (a) and CASE 2 (b).

other positions. The distribution of skewness values in CASE 1 and CASE 2 also differs. For instance, CASE 1 exhibits a skewness peak at $x = 61\text{m}$, while CASE 2 shows a skewness peak at $x = 67.5\text{m}$. Consequently, it is hypothesized that skewness may be connected to the stream velocity (Zhang and Zou, 2023).

4.2. Wave group propagation and wavelet analysis

According to the definition of skewness, the stream velocity of the wave field at different positions is also considered. The stream velocity of CASE1 is illustrated in Fig. 17, where the skewness at $x = 60\text{m}$ and $x = 61\text{m}$ is greater than that at $x = 64.5\text{m}$. In the flow field, it can be found that the velocity vectors at $x = 60\text{m}$ and $x = 61\text{m}$ along the propagation direction at wave crest are greater than those in $x = 64.5\text{m}$. Fig. 18 shows the stream velocity in CASE 2. The skewness value at $x = 67.5\text{m}$ is significant, with the velocity vector of the crest along the propagation direction having the largest value compared to the other two positions.

To analyze the evolution of freak waves, Fig. 19 depicts the progression of wave train propagation in the wave tank during the generation of CASE 1 and CASE 2. The red line connects the time and location at which the maximum wave height occurs in CASE 1, while the green line illustrates the temporal and spatial evolution of the maximum wave height in CASE 2. It is evident that as the waves evolve, the time of the

maximum wave height in each wave train moves progressively backward, exhibiting a pattern of dispersion-focusing-dispersion in space. Additionally, wave packets with smaller amplitudes emerge both before and after the maximum wave height wave, and gradually move closer to the focusing position.

The Wavelet Transform is employed to elucidate the development of energy in waves more plainly. In CASE 1, Fig. 20 depicts the wavelet energy spectra of the corresponding wave trains at four distinct wave probes. It can be observed that the energy is fairly dispersed, with the frequency concentrated in the initial stages of wave evolution (i.e., the location of the $x = 49.7\text{m}$). As the wave progresses and forms a freak wave, the energy gradually shifts towards the high frequency direction, taking on a triangular shape. Subsequently, as the wave moves away from the concentrated position, the high-frequency energy component gradually transitions to a low frequency, ultimately assuming a crescent-like form.

As depicted in Fig. 21 (a), the displacement of the high-frequency component with respect to both space and time is clearly discernible when the energy is concentrated at a magnified view in CASE1. Simultaneously, several low-energy regions with a broad range of frequencies are observed. These low-energy regions are generally uniform during the initial development of the wave and form a peak in the high-frequency region when the freak wave emerges. However, at $x = 67.5\text{m}$, the

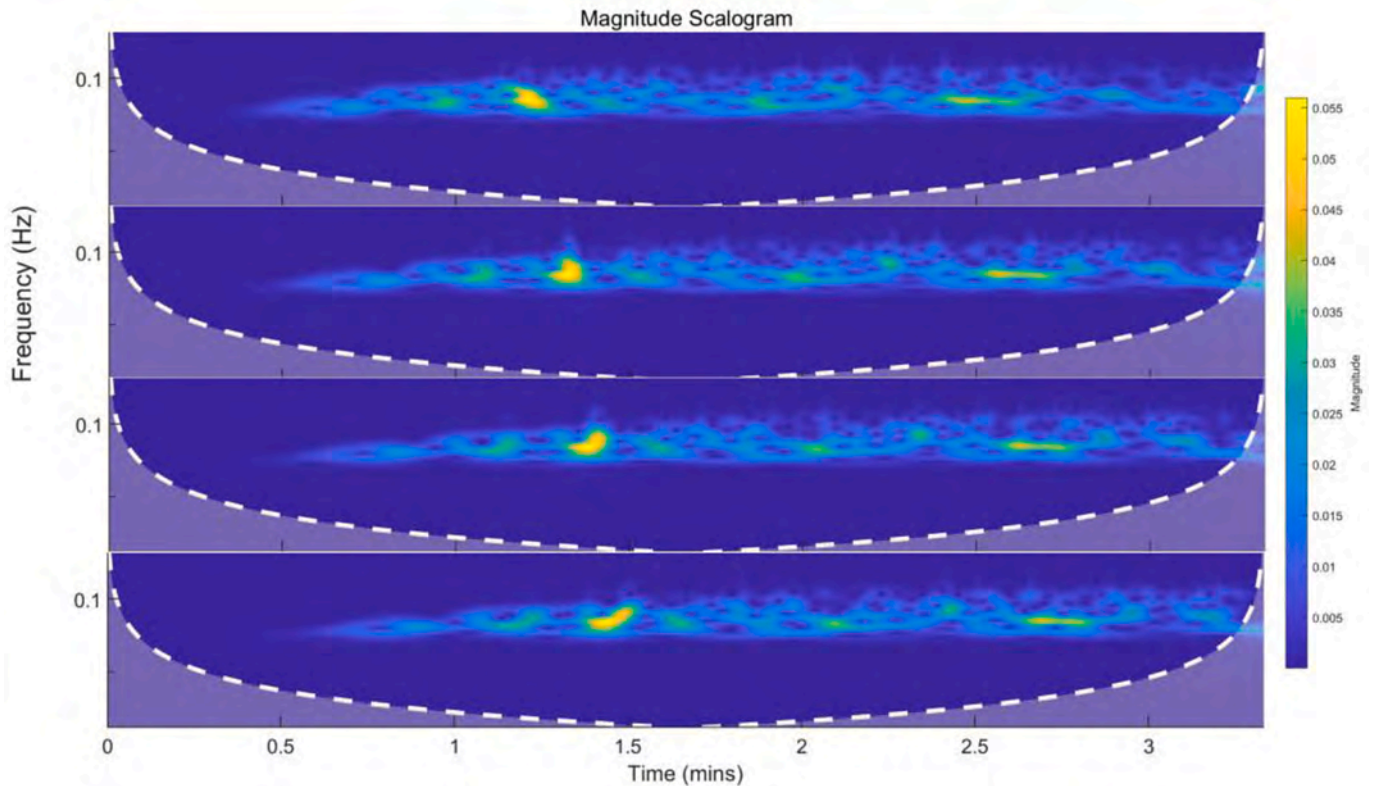


Fig. 20. The wavelet analysis of CASE1 in $x = 49.7\text{m}$, 60m , 64.5m and 67.5m (from top to bottom).

distribution of the low-energy region remains aligned with the high-energy region, presenting a blunted peak in the high frequency.

There exists a secondary high-energy region ahead from the main concentrated energy region in CASE 2. The secondary high-energy region dissipates with the propagation of the wave. Similar to that in CASE 1, the peak of the high-energy region moves backward with wave propagation. It can be observed that the occurrence of a freak wave is a situation of high-frequency wave component aggregates.

4.3. EMD analysis of freak waves

To quantitatively analyze the frequency and energy distribution of freak waves, the EMD (Empirical Mode Decomposition) method is utilized to decompose wave trains at various positions, as illustrated in Fig. 22. The red curve depicts the original time history curve of the wave train, which can be separated into the amplitude time history curve and energy concentration frequency corresponding to the components from order 1 to order 8. To facilitate comparison, the Fast Fourier Transform method is employed to evaluate the wave trains obtained from different measurement points of the same wave, as evident in Figs. 23 and 24.

The first four modes of wave decomposition are examined and analyzed, and four positions are selected the same with that in Section 4.3 during the wave evolution process. The results indicate that when waves evolve, the first mode of the wave remains consistent across different spatial locations, as demonstrated in Fig. 23(a). In the second mode, the frequencies of the four probes are not significantly different, but the amplitude in $x = 61\text{m}$ is greater than the other three locations. In the third mode, location $x = 64.5\text{m}$ has a higher amplitude. In the fourth mode, the amplitude in $x = 61\text{m}$ is the largest, and that in $x = 66\text{m}$ is the smallest. Overall, the amplitudes of the second mode and the fourth mode at the maximum kurtosis of CASE 1 are larger.

The distribution of modalities at four probes in CASE 2 is illustrated in Fig. 24, which corresponds to the same locations as that in Section 3.3. The first modes of the four locations have similar amplitudes and

frequencies. For the second modes, location $x = 72.1\text{m}$ and $x = 67.5\text{m}$ exhibit large amplitudes. In the third and fourth modes, the maximum amplitude position is $x = 62\text{m}$. It is evident that the dominant position of the second mode is behind the position of the maximum wave height in CASE 2.

The EMD analysis of CASE 1 and CASE 2 shows varying results. The position of $x = 61\text{m}$ in CASE 1 is higher in IMF2 and IMF3, while $x = 72.1\text{m}$ has larger value in IMF2 in CASE 2. These differences are due to the wave evolution process at different wave heights and periods. In Fig. 18, only one region of high energy appears in CASE 1, while CASE 2 has two kinds of regions. In the case of CASE1, this high-energy region occupies mid- and high-frequency proportions and therefore displays larger values in the first three modes. For CASE 2, the secondary high-energy region is slightly in the lower frequency range than that of the main high-energy region, and the energy decreases and moves towards the lower frequency region as the wave propagates. Therefore, the values of IMF2 and IMF3 at $x = 61\text{m}$ shows large value in CASE 1, while IMF2 at $x = 72.1\text{m}$ has large value in CASE 2.

5. Conclusions

In this paper, the nonlinear evolution and statistical characteristics of freak waves are studied, and two waves with different spectral peak periods and significant wave heights are analyzed. The freak waves are generated in a physical wave tank applying the two-wave train superposition method, and numerical simulations were carried out with potential theory (High-Order Spectral method) and viscous coupled method (HOS-CFD).

The accuracy of the HOS and HOS-CFD methods is verified, and the parameters for calculating freak waves with these two methods are analyzed. For the HOS method, settings of $M = 5$ and Nodes = 512 are found to be suitable for freak wave simulations. When using the HOS-CFD method, the grids in the viscous region are set to approximately 100 grids per wavelength and 14 grids per wave height.

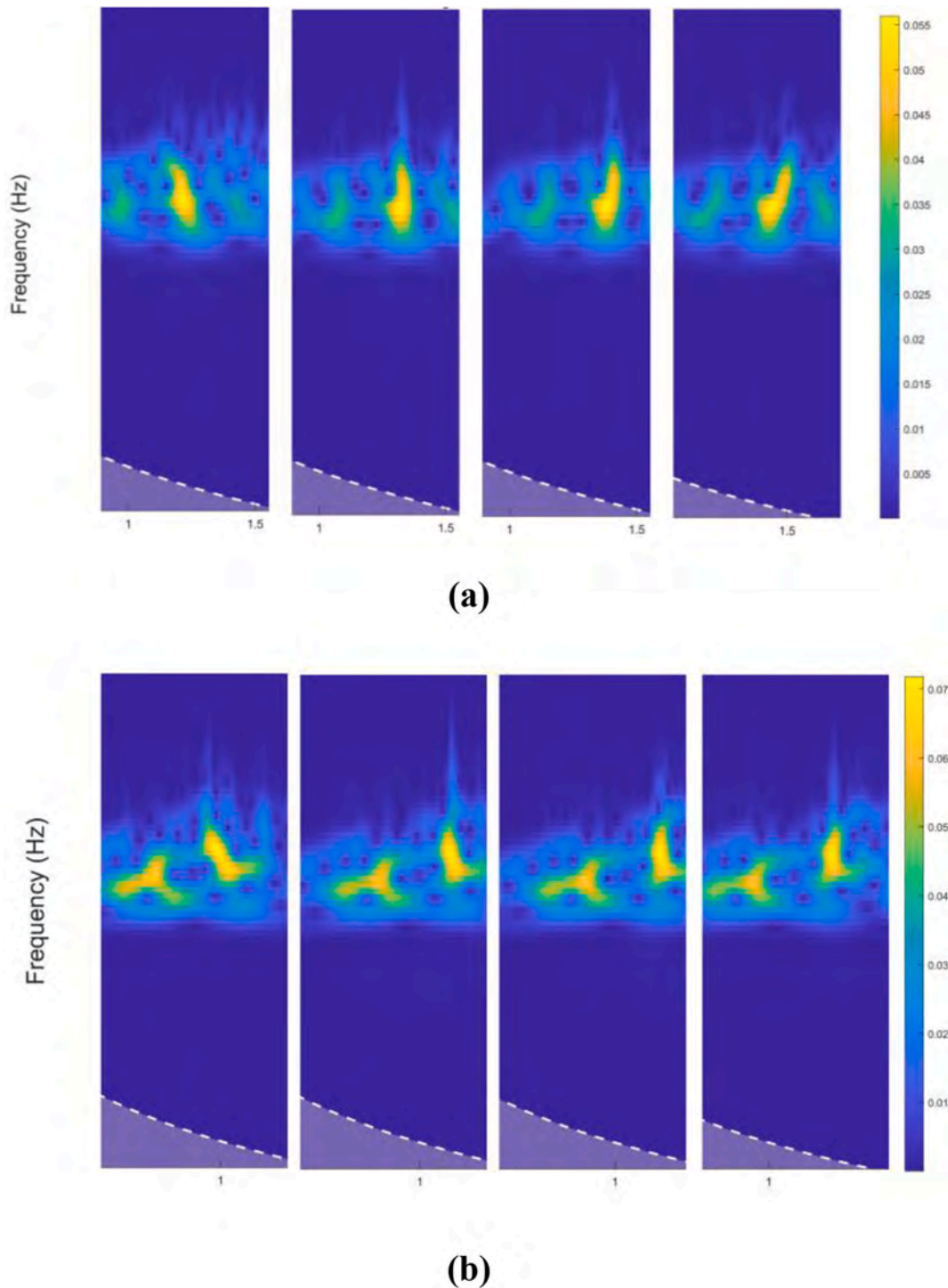


Fig. 21. The wavelet analysis of local energy in CASE1 (a) and CASE2 (b) in $x = 49.7\text{m}, 60\text{m}, 64.5\text{m}$ and 67.5m .

By analyzing the statistical characteristics of kurtosis and skewness of freak waves at different wave probes, new insights into the mechanisms of freak waves are obtained. Kurtosis is found to be closely related to the wave crest value. This indicates that kurtosis can serve as an important indicator to reflect the extreme nature of the wave crest in freak waves. A higher kurtosis value corresponds to a larger wave crest, which is a significant characteristic of freak waves.

Skewness, on the other hand, reflects two aspects of freak wave mechanisms. It not only indicates the position of the peak wave height but also is related to the velocity value at the wave crest in the propagation direction. A greater positive skewness value implies a larger

velocity component at the wave crest, making the wave more prone to breaking. This finding provides an understanding of the instability and potential hazards of freak waves during their propagation.

The Wavelet Transform and Empirical Mode Decomposition (EMD) methods are employed to analyze the propagation process of freak waves. In the process of freak wave propagation, high-frequency energy first converges, and when the freak wave is formed, the energy is distributed in a triangular shape along the time-frequency axis. As the maximum wave height decays during propagation, the high-frequency energy gradually disperses and decreases, eventually forming a lying crescent shape with high-energy region. Additionally, a low-energy

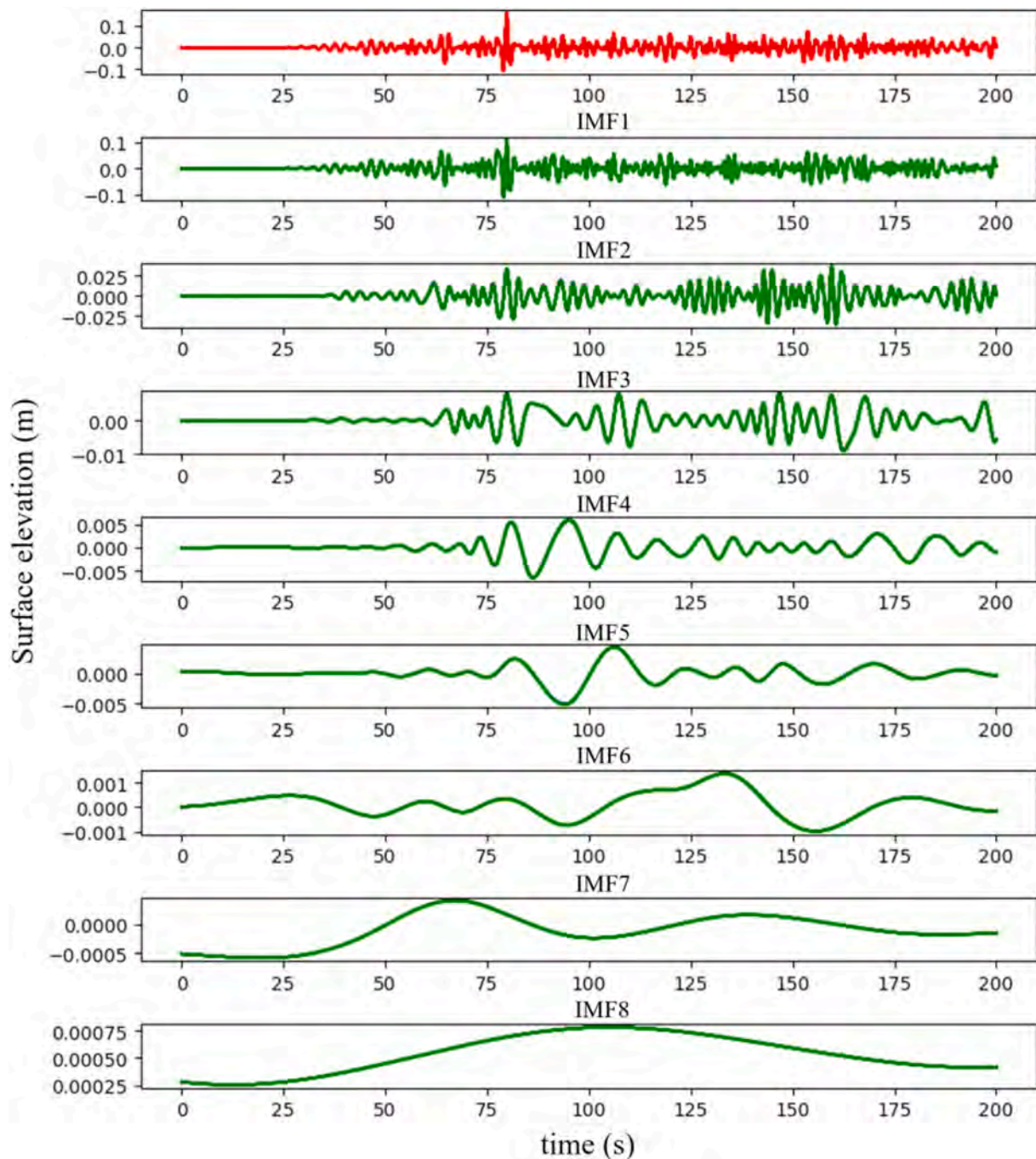


Fig. 22. The EMD analysis of wave elevation of probe 8 in CASE 1.

region with a wide frequency band exists during the propagation of freak waves, and it shows a peak when the freak wave is generated.

Through EMD analysis, different modal distributions were observed in CASE1 and CASE2. In CASE1, the second mode is the largest at the maximum skewness position, and the fourth mode is the largest at the position after the peak wave height occurred. In CASE2, the second and fourth modes are the largest after and before the maximum wave height occurred, respectively, and both show high-frequency characteristics. This reveals that the energy distribution and modal characteristics of freak waves are complex and related to their evolution process.

In summary, although energy accumulates at the position of the maximum wave height, there are often large amplitude modes in areas away from the location where the freak wave occurs. These can introduce low-frequency energy to marine structures, threatening production

and operation safety. In future research, the authors plan to simulate and analyze structures operating at different positions in freak waves and observe the hydrodynamic features in positions far from the peak position, further exploring the complex interactions between freak waves and marine structures.

CRediT authorship contribution statement

Yuan Zhuang: Writing – original draft, Visualization, Validation, Software, Methodology, Investigation, Formal analysis, Data curation, Conceptualization. **Yangjun Wang:** Writing – review & editing, Visualization, Validation, Formal analysis, Data curation. **Zhiben Shen:** Writing – review & editing, Validation, Formal analysis, Data curation. **Guohua Pan:** Validation, Formal analysis, Data curation. **Decheng**

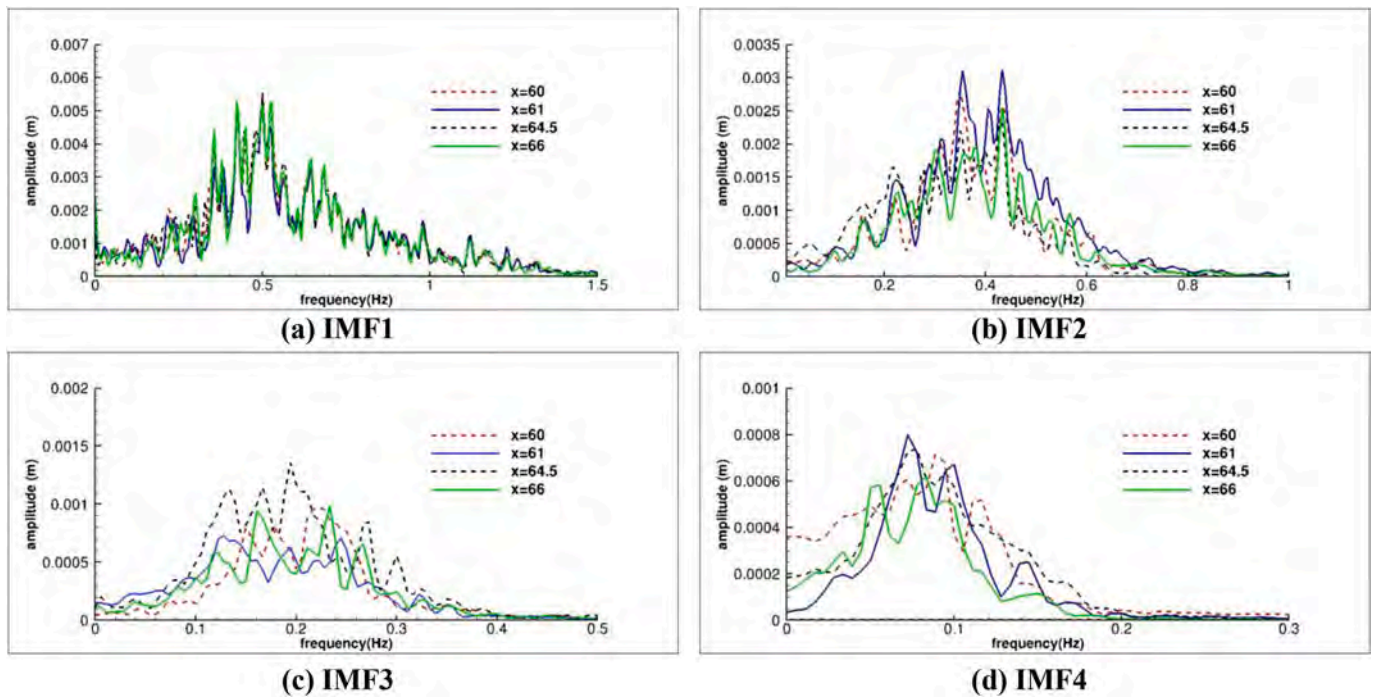


Fig. 23. The results of Intrinsic mode function (IMF) of four positions in CASE 1.

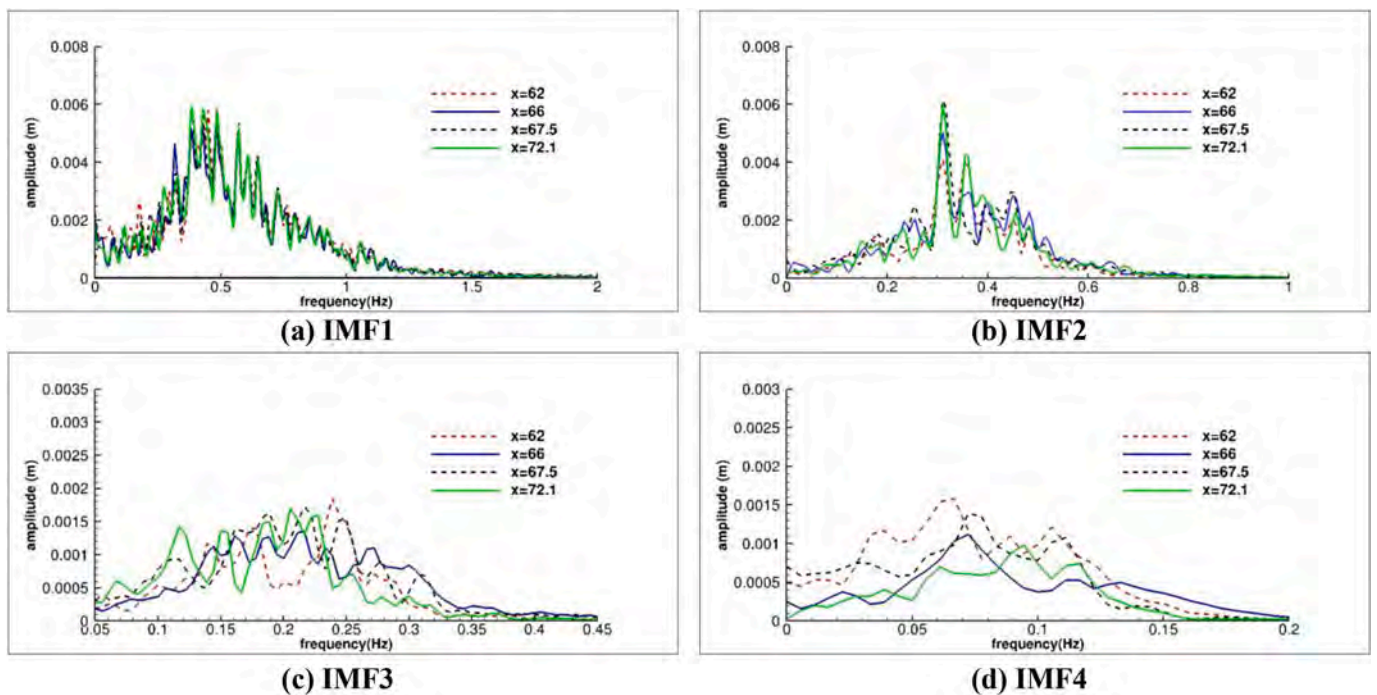


Fig. 24. The results of Intrinsic mode function of four positions in CASE 2.

Wan: Writing – review & editing, Supervision, Software, Project administration, Investigation, Funding acquisition, Conceptualization.

Data availability

The data that support the findings of this study are available from the corresponding author upon reasonable request.

Declaration of competing interest

The authors declare that they have no known competing financial interests or personal relationships that could have appeared to influence the work reported in this paper.

Acknowledgement

This work was supported by the National Natural Science Foundation

of China (52201372, 52131102), and sponsored by the Oceanic Interdisciplinary Program of Shanghai Jiao Tong University (project number SL2022PT106), to which the authors are most grateful.

References

- Abroug, I., Matar, R., Abcha, N., 2022. Spatial evolution of skewness and kurtosis of unidirectional extreme waves propagating over a sloping beach. *J. Mar. Sci. Eng.* 10 (10), 1475.
- Chabchoub, A., Hoffmann, N.P., Akhmediev, N., 2011. Rogue wave observation in a water wave tank. *Phys. Rev. Lett.* 106 (20), 204502.
- Chang, S., Huang, W., Liu, F., Song, H., 2021. Influence of second-order wave force and focusing position on dynamic responses of tension leg platform under a freak wave. *Ocean Eng.* 242, 110126.
- Deng, Y., Zhu, C., Wang, Z., 2024. Numerical study on modeling and local characteristics of a predetermined freak wave. *J. Offshore Mech. Arctic Eng.* 146 (1), 011203.
- Deng, Y.F., Yang, J.M., Tian, X.L., Li, X., Xiao, L.F., 2016. An experimental study on deterministic freak waves: generation, propagation and local energy. *Ocean Eng.* 118, 83–92.
- Ducrozet, G., Bingham, H.B., Engsig-Karup, A.P., Bonnefoy, F., Ferrant, P., 2012. A comparative study of two fast nonlinear free-surface water wave models. *Int. J. Numer. Methods Fluid.* 69 (11), 1818–1834.
- Ducrozet, G., Bonnefoy, F., Le Touzé, D., Ferrant, P., 2006. Implementation and validation of nonlinear wavemaker models in a HOS numerical wave tank. *Int. J. Offshore Polar Eng.* 16 (3).
- Ducrozet, G., Bonnefoy, F., Mori, N., Fink, M., Chabchoub, A., 2020. Experimental reconstruction of extreme sea waves by time reversal principle. *J. Fluid Mech.* 884, A20.
- Dysthe, K., Krogstad, H.E., Müller, P., 2008. Oceanic rogue waves. *Annu. Rev. Fluid Mech.* 40, 287–310.
- Hayer, S., Andersen, O.J., 2000. Freak waves: rare realizations of a typical population or typical realizations of a rare population? [C]. In: ISOPE International Ocean and Polar Engineering Conference. ISOPE, Seattle, USA. ISOPE-I-00-233.
- Houtani, H., Waseda, T., Fujimoto, W., Kiyomatsu, K., Tanizawa, K., 2015. Freak wave generation in a wave basin with HOSM-WG method [C]. In: International Conference on Offshore Mechanics and Arctic Engineering, vol. 56550. American Society of Mechanical Engineers. V007T06A085.
- Ji, X., Li, A., Li, J., Wang, L., Wang, D., 2022. Research on the statistical characteristic of freak waves based on observed wave data. *Ocean Eng.* 243, 110323.
- Khait, A., 2020. Third-order generation of narrow-banded wave trains by a wavemaker. *Ocean Eng.* 218, 108200.
- Kjeldsen, S.P., 2004. Measurements of freak waves in Norway and related ship accidents [C]. In: Proceedings of the Royal Institution of Naval Architects International Conference-Design and Operation for Abnormal Conditions III. London, UK.
- Kriebel, D.L., Alsina, M.V., 2000. Simulation of extreme waves in a background random sea [C]. The Tenth International Offshore and Polar Engineering Conference. ISOPE, Seattle, USA. ISOPE-I-00-219.
- Luo, M., Koh, C.G., Lee, W.X., Lin, P.Z., Reeve, D.E., 2020. Experimental study of freak wave impacts on a tension-leg platform. *Mar. Struct.* 74, 102821.
- Mori, N., Janssen, P.A.E.M., 2006. On kurtosis and occurrence probability of freak waves. *J. Phys. Oceanogr.* 36 (7), 1471–1483.
- Mori, N., Onorato, M., Janssen, P.A.E.M., 2011. On the estimation of the kurtosis in directional sea states for freak wave forecasting. *J. Phys. Oceanogr.* 41 (8), 1484–1497.
- Slunyaev, A., Didenkulova, I., Pelinovsky, E., 2011. Rogue waves in 2006–2010. *Nat. Hazards Earth Syst. Sci.* 11, 2913–2924.
- Sun, Z., Zhao, X., Zhang, Y., Shen, J., 2008. Focusing models for generating freak waves [C]. In: ISOPE Pacific/Asia Offshore Mechanics Symposium. ISOPE. ISOPE-P-08-002.
- Tian, Z., Perlin, M., Choi, W., 2011. Frequency spectra evolution of two-dimensional focusing wave groups in finite depth water. *J. Fluid Mech.* 688, 169–194.
- Tromans, P.S., Anaturk, A.R., Hagemeyer, P., 1991. A new model for the kinematics of large ocean waves-application as a design wave [C]. In: ISOPE International Ocean and Polar Engineering Conference. ISOPE. ISOPE-I-91-154.
- Trulsen, K., Raustøl, A., Jorde, S., Rye, L.B., 2020. Extreme wave statistics of long-crested irregular waves over a shoal. *J. Fluid Mech.* 882, R2.
- Wang, J., Qin, H., Hu, Z., Mu, L., 2023. Three-dimensional study on the interaction between a container ship and freak waves in beam sea. *Int. J. Nav. Archit. Ocean Eng.* 15, 1–19.
- Wang, L., Ding, K., Zhou, B., Jin, P., Liu, S., Wang, J., Tang, T., 2023. Nonlinear statistical characteristics of the multi-directional waves with equivalent energy. *Phys. Fluids* 35 (8).
- Wang, L., Zhou, B., Jin, P., Li, J., Liu, S., Ducrozet, G., 2022. Relation between occurrence probability of freak waves and kurtosis/skewness in unidirectional wave trains under single-peak spectra. *Ocean Eng.* 248, 110813.
- Xu, P., Zhang, Z., Li, S., Song, Q., Liu, W., 2024. Numerical investigation into the dynamic responses of floating photovoltaic platform and mooring line structures under freak waves. *J. Mar. Sci. Eng.* 12 (1), 96.
- Xue, S., Xu, G., Xie, W., Xu, L., Jiang, Z., 2023. Characteristics of freak wave and its interaction with marine structures: a review. *Ocean Eng.* 287, 115764.
- Zeng, H., Trulsen, K., 2012. Evolution of skewness and kurtosis of weakly nonlinear unidirectional waves over a sloping bottom. *Nat. Hazards Earth Syst. Sci.* 12 (3), 631–638.
- Zhang, J., Benoit, M., Kimmoun, O., Chabchoub, A., Hsu, H.C., 2019. Statistics of extreme waves in coastal waters: large scale experiments and advanced numerical simulations. *Fluid* 4 (2), 99.
- Zhang, Y., Zou, Z., 2023. A new expression for free stream velocity with skewness and asymmetry. *Ocean Eng.* 268, 113386.
- Zhao, X., Ye, Z., Fu, Y., Cao, F., 2014. A CIP-based numerical simulation of freak wave impact on a floating body. *Ocean Eng.* 87, 50–63.
- Zhuang, Y., Wan, D., 2021. Parametric study of a new HOS-CFD coupling method. *J. Hydrodyn.* 33 (1), 43–54.
- Zhuang, Y., Wang, G., Wan, D., Wu, J., 2022. Numerical simulations of FPSO with sloshing tanks in a random freak waves. *J. Hydrodyn.* 34 (3), 491–498.
- Zhuang, Y., Zhao, W., Wan, D., 2023. The nonlinearity of scattering waves due to interaction between focusing waves and floating production storage and offloading. *Phys. Fluids* 35, 107113.
- Zou, L., Wang, A., Wang, Z., Pei, Y., Liu, X., 2019. Experimental study of freak waves due to three-dimensional island terrain in random wave. *Acta Oceanol. Sin.* 38, 92–99.